

The Investigation of Backscattering Characteristics of 3-D Local Sea Surface with Time-varying Overturning Wave Crest

X. Meng¹, L. X. Guo², S. R. Chai², and Y. C. Jiao¹

¹National Key Laboratory of Antennas and Microwave Technology
Xidian University, Xi'an, Shaanxi 710071, China
mengxxidian@126.com

²School of Physics and Optoelectronic Engineering
Xidian University, Xi'an, Shaanxi 710071, China
lxguo@xidian.edu.cn, srchai1989@gmail.com, ychjiao@xidian.edu.cn

Abstract —When there exists overturning wave crest on the sea surface, the sophisticated coupling effect between the overturning wave crest and sea surface may give rise to sea spikes. As sea spikes will cause the increase of radar false probability, the investigation of electromagnetic (EM) scattering characteristics of three-dimensional (3-D) local sea surface with time-varying overturning wave crest is meaningful for the remote sensing. In this paper, the influence of wind speed and time factor is taken into consideration when constructing the overturning wave crest, which is ignored in the traditional Longtank model. In addition, the Integral Equation Method (IEM) is adopted to calculate the EM scattering from a 3-D local sea surface with time-varying overturning wave crest for different incident angles and wind speeds. The simulation results are meaningful for analyzing the physical mechanism of sea spikes.

Index Terms — IEM, sea spikes, time-varying overturning wave crest.

I. INTRODUCTION

The sea spikes, which may cause the increase of radar false probability, have been hot issues during the past decades [1-6]. HH signals exceeding VV signals by as much as 10 dB or more is one of the characteristics of sea spikes. The overturning wave crest is thought to be a main reason to sea spikes, where the sophisticated coupling effect between sea surface and overturning wave crest may give rise to sea spikes. Therefore, the investigation of EM scattering from the 3-D local sea surface with time-varying overturning wave crest is of great importance for the physical mechanism analysis of sea spikes.

The Longtank model [7] has been widely used for the study of physical mechanism of sea spikes [3-5], which is generated by the University of California at Santa Barbara. The Longtank model is a series of

numerically generated wave profiles, representing different profiles of overturning wave crest. These previous works indicated that multiple scattering from the crest and the front face of the overturning wave crest and the Brewster angle effect are the main reasons to HH signals exceeding that of VV signals. Actually, the multiple scattering also takes place between the sea surface and overturning wave crest. Therefore, it is necessary to investigate the EM scattering from the 3-D local sea surface with overturning wave crest. As the profile of sea surface is related to the wind speed, in order to combine the overturning wave crest with the generated sea surface, the wind speed should be taken into account when modeling. However, the Longtank model didn't consider the influence of wind speed. Therefore, the time-varying overturning wave crest model is applied to make a combination with the 3-D local sea surface in this paper, whose length and height are related to the wind speed and time factor. The 3-D sea surface is constructed by the Monte Carlo [8] method. Finally, the 3-D local sea surface with time-varying overturning wave crest can be built by the boolean operation, where the interpolation operation is adopted to avoid the discontinuity of the boundary.

To deal with the EM scattering from the 3-D local sea surface with time-varying overturning wave crest, the IEM [9]—an approximate method, is applied as a result of the limitation of numerical techniques [10-13] on the computer resource. The backscattering RCS and scattered electric field ratio of the 3-D local sea surface with overturning wave crest at different time sampling points are compared in detail. Meanwhile, the influence of wind speed on the backscattering characteristics is analyzed. Furthermore, the influence of overturning wave crest on the scattering characteristics of sea surface as well as the physical mechanism of sea spikes is also discussed. Compared with the previous literatures, our work focused on the variation of EM scattering of 3-D

local sea surface with overturning wave crest during the generation process, giving a detail analysis of sea spikes.

II. THEORY AND FORMULATION

In this section, a detailed description of the construction of 3-D local sea surface with overturning wave crest will be presented. Meanwhile, the EM scattering from the models was found using the IEM.

A. Time-varying overturning wave crest model

The two-dimensional (2-D) overturning wave crest is shown in Fig. 1, whose length and height are represented by H and L , respectively.

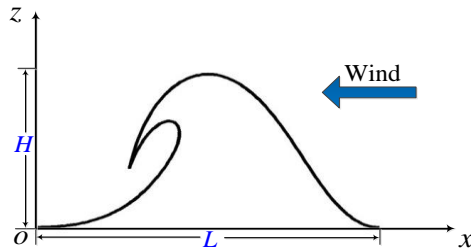


Fig. 1. The 2-D overturning wave crest.

According to [14], the height of wave is related to the wind speed, which can be expressed as:

$$H = 17.03 \cdot \exp\left(-\frac{\alpha^2}{18.3269}\right) + 2.361 \cdot \exp\left(-\frac{\beta^2}{8.8646}\right), \quad (1)$$

where $\alpha = u^{2/3} - 12.6549$, u is the wind speed.

S is defined as $S = H / L$. Therefore, the length of wave can be achieved by $L = H / S$.

The overturning wave crest takes place over a wide range of temporal and spatial scales. Therefore, the time factor is included to control its profile,

$$\begin{cases} x = L \cdot ((0.5 - s_1) \cos(\phi) - r \sin(\phi) + 0.5) \\ z = H \cdot z' / z_{\max} = H [(0.5 - s_1) \sin(\phi) + r \cos(\phi)] k_7 / z_{\max} \end{cases}, \quad (2)$$

$$\begin{cases} s_1 = \frac{(2s)^{k_1}}{2} \quad (0 \leq s \leq 0.5), \\ s_2 = (2s)^{k_2} \end{cases}, \quad \begin{cases} s_1 = \frac{1 + (2s - 1)^{k_1}}{2} \quad (0.5 \leq s \leq 1), \\ s_2 = 1 - (2s - 1)^{k_1} \end{cases}, \quad (3)$$

where $s(0 \leq s \leq 1)$ is the input space parameter, which is splitted for the front and back of overturning wave crest. $k_1 \sim k_7$ can be obtained in [14]. It should be noted that k and s are related to the time factor, therefore the profile of overturning wave crest varies with time stepping.

$r = k_2(1 + \cos((s_2 - 1)\pi)) / 2 + k_3 s_2^{k_4}$, $\phi = \pi k_5 s_2^{k_6} / 2$, $z_{\max} = \max\{z'\}$, and the period of overturning wave crest is $T = 2s$.

In this paper, the time-varying overturning wave crest model is obtained at sixteen different time sampling

points as shown in Fig. 2. The wind speeds are $u = 5\text{m/s}$ and $u = 7\text{m/s}$, respectively. The direction of wind is along with $-x$ axis and $S = 1/3$. The time sampling interval is $\Delta t = 0.9 / 15(\text{s})$.

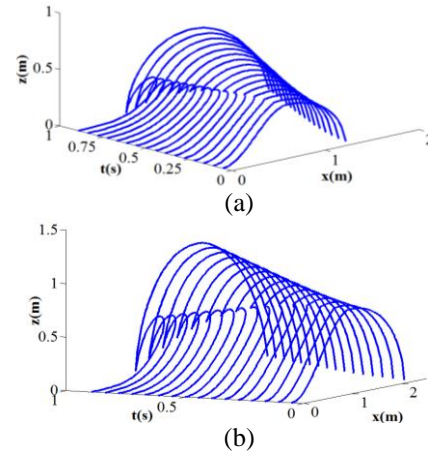


Fig. 2. The 2-D overturning wave crest for different wind speeds: (a) $u = 5\text{m/s}$ and (b) $u = 7\text{m/s}$.

As illustrated in Fig. 2, the profiles of overturning wave crest are obtained at sixteen time sampling points, which represented the temporal evolution of overturning wave crest. The height and length of overturning wave crest increased with wind speed. In addition, the overturning wave crest begins to generate at $t = \Delta t$, therefore its height and length are the smallest, which reached the maximum at $t = 16\Delta t$. When the 2-D time-varying overturning wave crest is constructed, the corresponding 3-D model can be achieved by extending the 2-D model in azimuth direction.

B. Construction of a 3-D local sea surface with overturning wave crest

The 3-D sea surface is modeled by the Monte Carlo method, where the Elfouhaily spectrum [15] is chosen to model the sea surface. The profiles of 3-D time-varying overturning wave crest are generated as described above. Then the 3-D overturning wave crest is combined with the 3-D sea surface by the boolean operation to build the composite model. In addition, the interpolation operation is adopted at the boundary between sea surface and overturning wave crest, avoiding the discontinuity at the boundary.

Figure 3 and Fig. 4 showed the 3-D local sea surface with overturning wave crest model at $t = \Delta t, 10\Delta t, 14\Delta t, 16\Delta t$. The wind speeds are $u = 5\text{m/s}$ and $u = 7\text{m/s}$. As presented in Figs. 3 and 4, these are simplified models due to the complexity of the real overturning wave crest, which can briefly describe the temporal evolution of the 3-D sea surface with overturning wave crest.

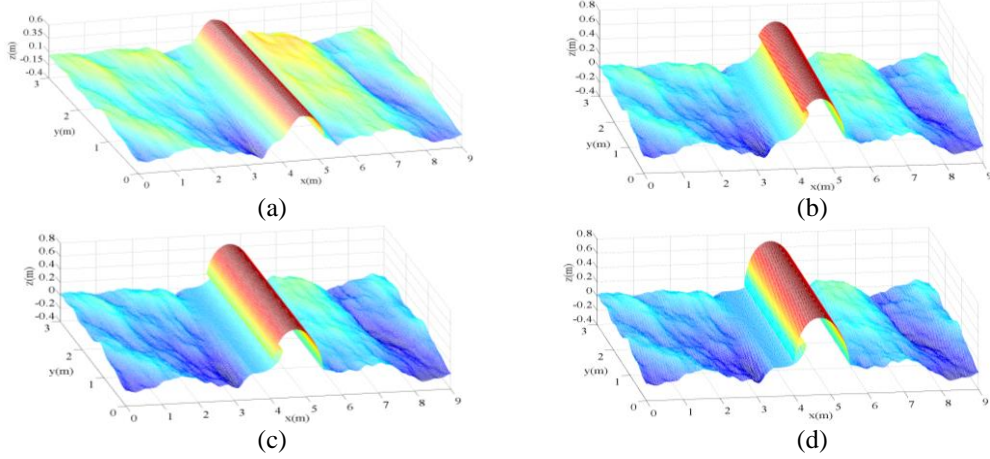


Fig. 3. The 3-D local sea surface with overturning wave crest ($u = 5\text{m/s}$): (a) Δt , (b) $10\Delta t$, (c) $14\Delta t$, and (d) $16\Delta t$.

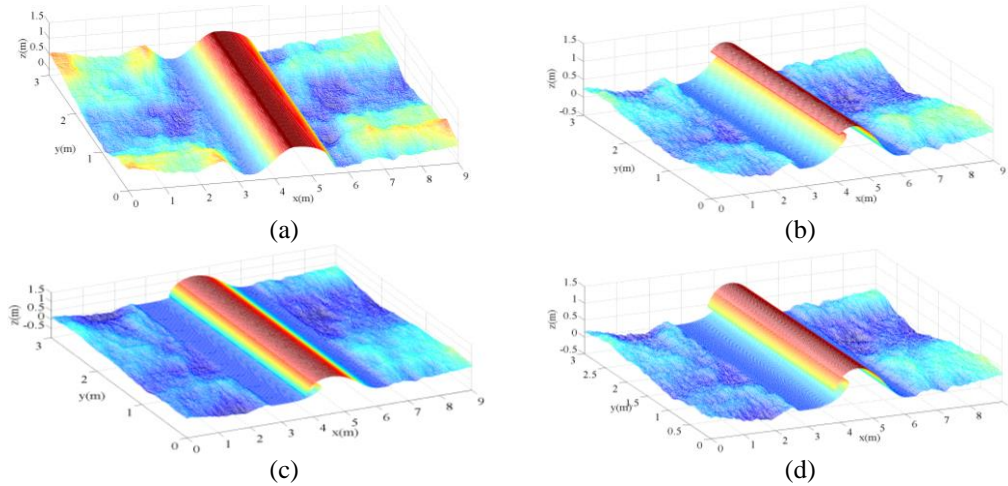


Fig. 4. The 3-D local sea surface with overturning wave crest ($u = 7\text{m/s}$): (a) Δt , (b) $10\Delta t$, (c) $14\Delta t$, and (d) $16\Delta t$.

C. IEM for the 3-D local sea surface with time-varying overturning wave crest

For the IEM, the governing equations for the tangential surface fields on a dielectric surface can be written as the sum of the standard Kirchhoff surface field and a complementary surface field,

$$\begin{cases} \hat{\mathbf{n}} \times \mathbf{E} = (\hat{\mathbf{n}} \times \mathbf{E})_k + (\hat{\mathbf{n}} \times \mathbf{E})_c \\ \hat{\mathbf{n}} \times \mathbf{H} = (\hat{\mathbf{n}} \times \mathbf{H})_k + (\hat{\mathbf{n}} \times \mathbf{H})_c \end{cases} \quad (4)$$

The standard Kirchhoff surface field and the complementary surface field can be expressed as:

$$(\hat{\mathbf{n}} \times \mathbf{E})_k = \hat{\mathbf{n}} \times [(1 + R_\perp)(\hat{\mathbf{p}} \cdot \hat{\mathbf{t}})\hat{\mathbf{t}} + (1 - R_\parallel)(\hat{\mathbf{p}} \cdot \hat{\mathbf{d}})\hat{\mathbf{d}}]E^i, \quad (5)$$

$$\eta(\hat{\mathbf{n}} \times \mathbf{H})_k = \hat{\mathbf{n}} \times [(1 - R_\perp)(\hat{\mathbf{p}} \cdot \hat{\mathbf{t}})\hat{\mathbf{d}} - (1 + R_\parallel)(\hat{\mathbf{p}} \cdot \hat{\mathbf{d}})\hat{\mathbf{t}}]E^i \quad (6)$$

$$= \hat{\mathbf{n}} \times \{\mathbf{k}_i \times [(1 - R_\perp)(\hat{\mathbf{p}} \cdot \hat{\mathbf{t}})\hat{\mathbf{t}} + (1 + R_\parallel)(\hat{\mathbf{p}} \cdot \hat{\mathbf{d}})\hat{\mathbf{d}}]E^i\},$$

$$(\hat{\mathbf{n}} \times \mathbf{E})_c = -\frac{1}{4\pi}(\hat{\mathbf{n}} \times \hat{\mathbf{t}})\{\hat{\mathbf{n}} \times \hat{\mathbf{t}} \cdot \hat{\mathbf{n}} \times \int [(1 + R_\perp)\boldsymbol{\varepsilon} +$$

$$(1 - R_\perp)\boldsymbol{\varepsilon}_i]ds'\} - \frac{1}{4\pi}\hat{\mathbf{t}}\{\hat{\mathbf{t}} \cdot \hat{\mathbf{n}} \times \int [(1 - R_\parallel)\boldsymbol{\varepsilon} + (1 + R_\parallel)\boldsymbol{\varepsilon}_i]ds'\}, \quad (7)$$

$$(\hat{\mathbf{n}} \times \mathbf{H})_c = \frac{1}{4\pi}(\hat{\mathbf{n}} \times \hat{\mathbf{t}})\{\hat{\mathbf{n}} \times \hat{\mathbf{t}} \cdot \hat{\mathbf{n}} \times \int [(1 + R_\parallel)\mathbf{h} +$$

$$(1 - R_\parallel)\mathbf{h}_i]ds'\} + \frac{1}{4\pi}\hat{\mathbf{t}}\{\hat{\mathbf{t}} \cdot \hat{\mathbf{n}} \times \int [(1 - R_\perp)\mathbf{h} + (1 + R_\perp)\mathbf{h}_i]ds'\}, \quad (8)$$

where $\hat{\mathbf{n}}$ is the unit normal vector of surface, R_\perp, R_\parallel are the Fresnel reflection coefficient, θ_i is incident angle.

$$\begin{cases} \hat{\mathbf{t}} = (\hat{\mathbf{k}}_i \times \hat{\mathbf{n}}) / |\hat{\mathbf{k}}_i \times \hat{\mathbf{n}}| \\ \hat{\mathbf{d}} = \hat{\mathbf{k}}_i \times \hat{\mathbf{t}} \\ \hat{\mathbf{k}}_i = \hat{\mathbf{t}} \times \hat{\mathbf{d}} \end{cases}, \quad (9)$$

$$\boldsymbol{\varepsilon} = jk\eta(\hat{\mathbf{n}}' \times \mathbf{H}')G - (\hat{\mathbf{n}}' \times \mathbf{E}') \times \nabla' G - (\hat{\mathbf{n}}' \cdot \mathbf{E}')\nabla' G, \quad (10)$$

$$\mathbf{h} = (jk / \eta)(\hat{\mathbf{n}}' \times \mathbf{E}')G + (\hat{\mathbf{n}}' \times \mathbf{H}') \times \nabla' G + (\hat{\mathbf{n}}' \cdot \mathbf{E}')\nabla' G, \quad (11)$$

$$\boldsymbol{\varepsilon}_i = -[jk\eta_i(\hat{\mathbf{n}}' \times \mathbf{H}')G_i - (\hat{\mathbf{n}}' \times \mathbf{E}') \times \nabla' G_i - (\hat{\mathbf{n}}' \cdot \mathbf{E}')\nabla' G_i / \varepsilon_i], \quad (12)$$

$$\mathbf{h}_i = -[\frac{jk_i}{\eta_i}(\hat{\mathbf{n}}' \times \mathbf{E}')G_i + (\hat{\mathbf{n}}' \times \mathbf{H}') \times \nabla' G_i + (\hat{\mathbf{n}}' \cdot \mathbf{H}')\nabla' G_i / \mu_i]. \quad (13)$$

where $\hat{\mathbf{t}}, \hat{\mathbf{d}}, \hat{\mathbf{k}}_i$ are the local coordinate vectors, $\hat{\mathbf{n}}, \hat{\mathbf{n}}'$ is the unit normal vector of the surface, G is the Green's

function, ε_r, μ_r are the ratios of the permittivity and permeability of medium 2 to medium 1.

For the scattering of a 3-D local sea surface with time-varying overturning wave crest by IEM, the model is meshed into a great deal of triangles. For each lighted triangle, its Kirchhoff surface field and complementary surface field can be obtained according to Equation (5)~(13). The complementary surface field is a sum of the complementary surface field from the other lighted triangles, which represented the coupling scattering from the other triangles. In the end, the scattered far fields are calculated by Stratton-Chu integral equation.

III. NUMERICAL RESULTS AND ANALYSIS

Firstly, the backscattering RCS of a 3-D local sea surface with overturning wave crest by IEM is compared with that of MoM in Fig. 5. The sea surface is $9\text{m} \times 3\text{m}$, and $u = 5\text{m/s}$. The overturning wave crest is obtained at $t = 8\Delta t$. The frequency is $f = 0.456\text{GHz}$. The incident angle θ_i varies from -90° to 90° , and the incident vector is in xoz plane. When θ_i varied from -90° to 0° , it means upwind incidence, and 0° to 90° means downwind incidence. The relative permittivity of the sea water is $\varepsilon_r = (72.942, 178.609)$, which is obtained by the Debye model [16]. As seen in Fig. 5 (b), the backscattering RCS of 3-D local sea surface with overturning wave crest by the IEM shows a great agreement with that of MoM. Therefore, the validation of IEM is proved.

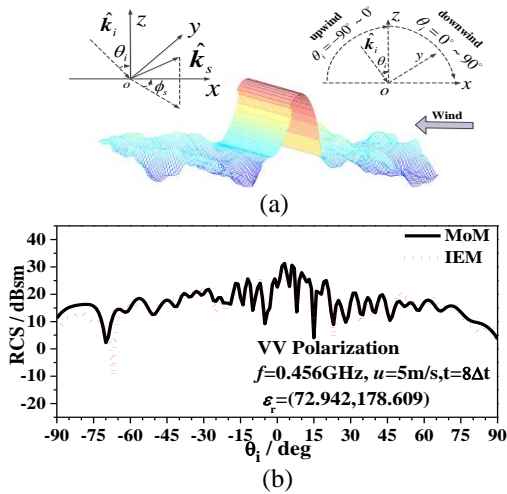


Fig. 5. Backscattering of a 3-D local sea surface with overturning wave crest: (a) model and (b) simulation results.

Figure 6 and Fig. 7 showed the backscattering RCS of a 3-D local sea surface with overturning wave crest by IEM for different wind speeds. Four profiles of overturning wave crest at $t = \Delta t$, $10\Delta t$, $14\Delta t$, $16\Delta t$ are

considered. The sea surface is $9\text{m} \times 3\text{m}$. The frequency of incident plane wave is $f = 0.456\text{GHz}$, and the relative permittivity is $\varepsilon_r = (72.942, 178.609)$. The incident vector is in xoz plane.

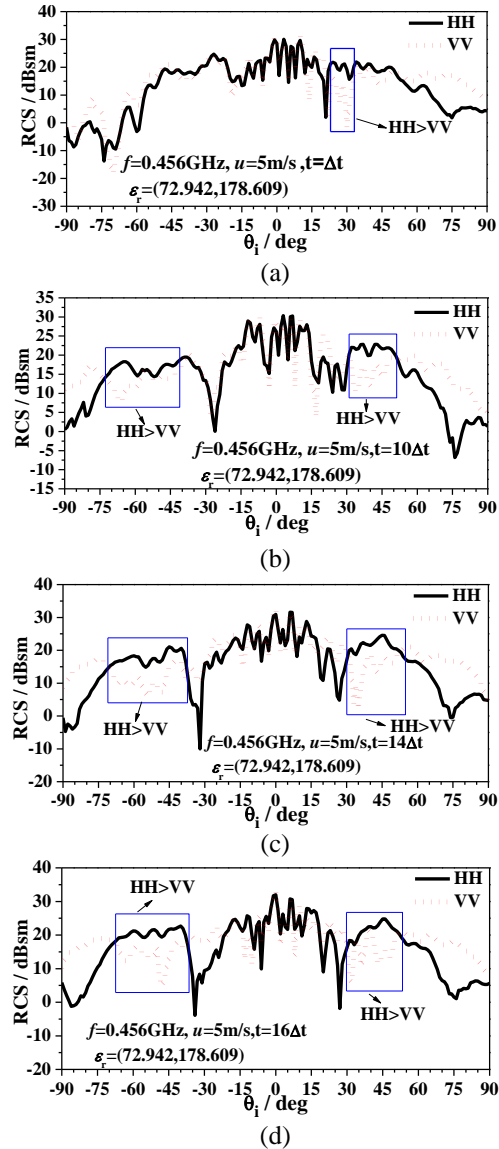


Fig. 6. Backscattering RCS for a 3-D local sea surface with overturning wave crest ($f = 0.456\text{GHz}$, $u = 5\text{m/s}$): (a) Δt , (b) $10\Delta t$, (c) $14\Delta t$, and (d) $16\Delta t$.

As shown in Fig. 6 the length and height of overturning wave crest are relatively smaller at the beginning of generation ($t = \Delta t$). Therefore, the sea surface scattering plays a major role, and backscattering RCS of HH polarization exceeding that of VV polarization is not observed except for $\theta_i = 20^\circ \sim 30^\circ$. However, the size of the overturning wave crest increased with time stepping, and its profile becomes

steeper. There is more incident angles for which HH scattering exceeding that of VV is observed. It is found that the sea-spike phenomenon is more likely to occur for upwind and large incident angle.

It can be seen from Fig. 7 that the backscattering RCS of HH polarization exceeding that of VV polarization becomes more obvious compared with that of $u = 5\text{m/s}$. The multiple scattering between the sea surface and overturning wave crest has a stronger contributor to the backscattering with the time stepping due to the increase of the size of overturning wave crest. Therefore, backscattering RCS of HH polarization

exceeding that of VV polarization can be observed for the upwind and large incident angles, where the difference between HH and VV polarizations is larger than that of $u = 5\text{m/s}$. Meanwhile, this phenomenon also occurred for some incident angles when the incident wave is along with the downwind direction, but the difference is much smaller than that of upwind incidence. This means that the sea spikes are more likely to take place for the upwind incidence especially for the strong sea spikes, which is mainly caused by the multiple scattering between the sea surface and the overturning wave crest.

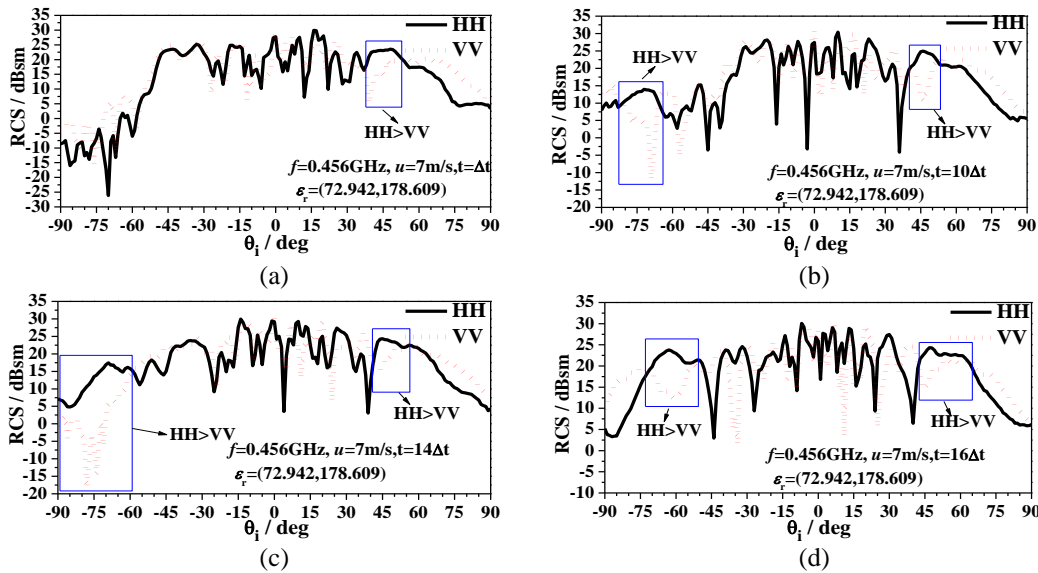


Fig. 7. Backscattering RCS for a 3-D local sea surface with overturning wave crest ($f = 0.456\text{GHz}$, $u = 7\text{m/s}$): (a) Δt , (b) $10\Delta t$, (c) $14\Delta t$, and (d) $16\Delta t$.

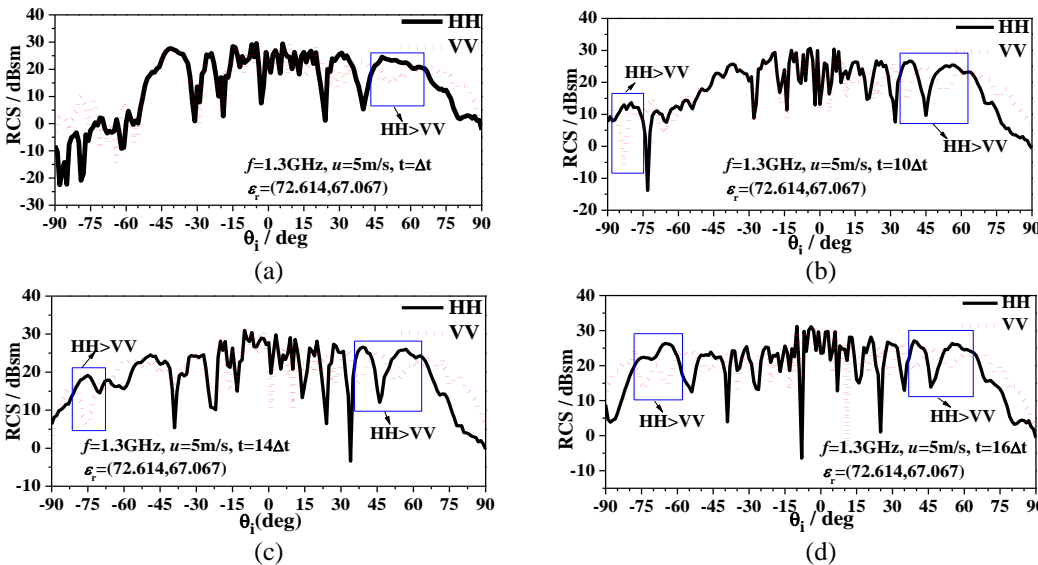


Fig. 8. Backscattering RCS for a 3-D local sea surface with overturning wave crest ($f = 1.3\text{GHz}$, $u = 5\text{m/s}$): (a) Δt , (b) $10\Delta t$, (c) $14\Delta t$, and (d) $16\Delta t$.

Figure 8 and Fig. 9 presented the backscattering RCS for $f = 1.3\text{GHz}$. The relative permittivity of the sea water is $\epsilon_r = (72.614, 67.067)$, which is also obtained by the Debye model [16].

According to the simulation results from Fig. 8, it can be seen that when the profiles of the overturning wave crest model became steeper, the backscattering RCS of HH polarization larger than that of VV polarization becomes more obvious, and this is agree with that in Fig. 5. Therefore, it demonstrated that the overturning wave crest has a strong contributor to the backscattering from the sea surface and are particularly responsible for sea spikes. It should be noted that although overturning wave crest is a main reason to sea spikes, but not the sufficient condition, which is also related to the included angle of the overturning wave crest and sea surface as well as the incident angle.

As shown in Fig. 9, the backscattering RCS varies more quickly with the increase of radar frequency, compared with that in Fig. 6. The scattering of the sea surface has a main contributor to the backscattering RCS at $t = \Delta t$, then the RCS of VV polarization is larger than that of HH polarization. The RCS of HH polarization exceeding that of VV polarization occurred with the time stepping. At $t = 10\Delta t, 14\Delta t, 16\Delta t$, this phenomenon can be observed for the upwind and large incident angles, where the difference between the HH polarization and VV polarization reaches as much as 20 dBsm or more at $t = 14\Delta t$. Compared with the results in Fig. 6, the roughness of the sea surface and the size of the overturning wave crest increase with the wind speed. Therefore, the multiple scattering is more serious as well as the phenomenon of RCS of HH polarization exceeding the VV polarization.

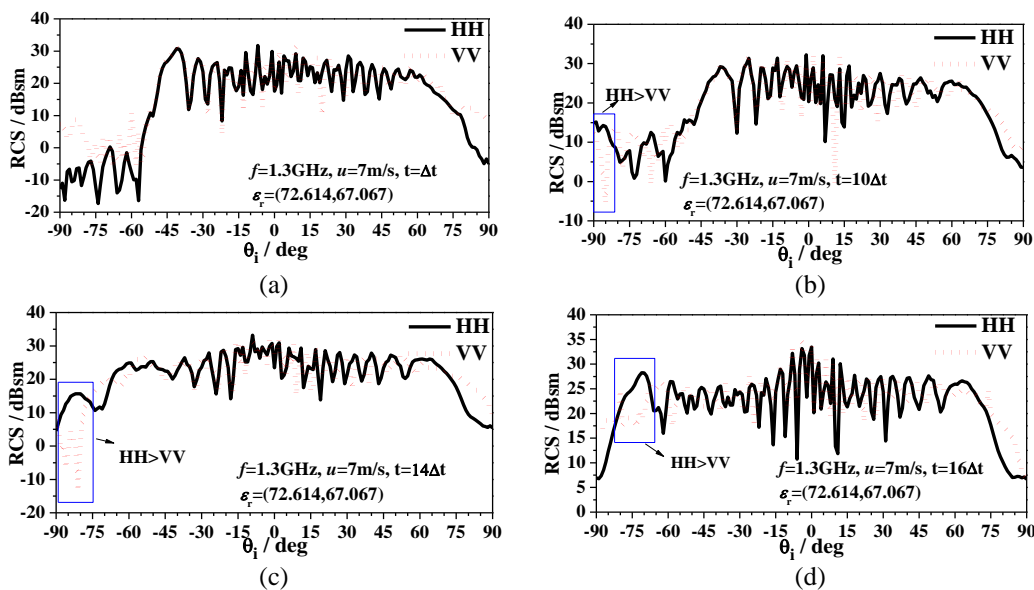


Fig. 9. Back scattering RCS for a 3-D local sea surface with overturning wave crest ($f = 1.3\text{GHz}$, $u = 7\text{m/s}$): (a) Δt , (b) $10\Delta t$, (c) $14\Delta t$, and (d) $16\Delta t$.

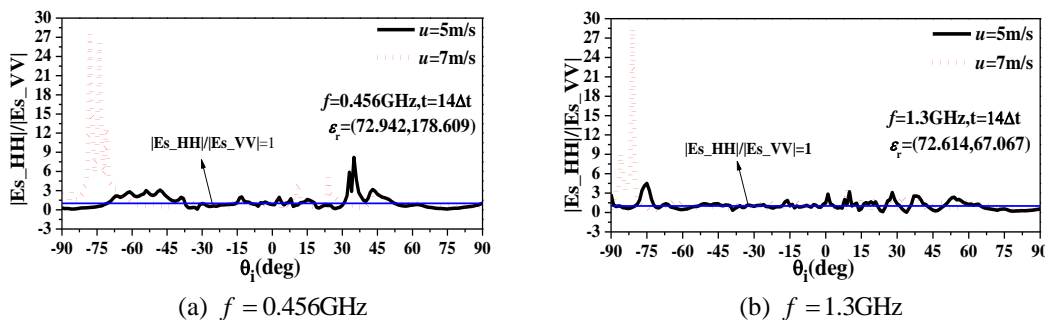


Fig. 10. Backscattering electric field ratio: (a) $f = 0.456\text{GHz}$ and (b) $f = 1.3\text{GHz}$.

The backscattering electric field ratio at $t=14\Delta t$ with different wind speeds and frequencies is depicted in Fig. 10. The blue line represents that the backscattering electric field ratio is equal to 1.

According to the simulation results in Fig. 10, with the increase of wind speed, there is more incident angles for which the strong sea-spike phenomenon is observed. Besides, a strong sea-spike phenomenon occurred for the incident angle between -90° and -65° , where the backscattering electric field ratio has nearly reached as much as 30. Therefore, it means that the strong sea spikes are more likely to take place for the upwind incidence, where the multiple scattering is more serious than that of the downwind incidence.

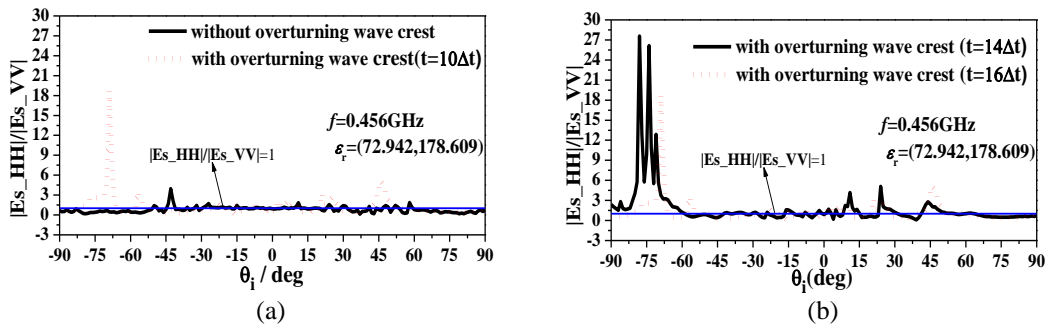


Fig. 11. Backscattering electric field ratio: (a) without/with overturning wave crest ($t = 10\Delta t$), and (b) sea surface with overturning wave crest ($t = 14\Delta t, 16\Delta t$).

IV. CONCLUSION

In this paper, the EM scattering characteristics of the 3-D local sea surface with the time-varying overturning wave crest is investigated based on IEM, where the overturning wave crest model is related to the wind speed and the time factor. The simulation results indicated that the overturning wave crest is particularly responsible for sea spikes. The size and profile of overturning wave crest also have a great influence on the backscattering RCS. When the length and height of overturning wave crest are relatively smaller at $t = \Delta t$, the sea surface scattering plays a domain role, and the sea-spike phenomenon is hardly to occur. While with the increase of the length and height of the overturning wave crest, the multiple scattering becomes obvious. When the incident angle is close to the Brewster angle of the sea water dielectric, the VV multipath is greatly attenuated and results in the sea spikes. According to the simulation results, the sea spikes are more easily to be observed for the upwind and large incident angles illumination. In addition, it should be noted that, as a result of the difficulty in the construction of real 3-D overturning wave crest, the 3-D local sea surface with overturning wave crest in this paper is a simplified model. Based on the present work, the further study will be carried on a

The comparison of backscattering electric field ratio from a 3-D local sea surface with and without the overturning wave crest is presented in Fig. 11, where the overturning wave crest are obtained at three different time sampling points and represents three different profiles of the overturning wave crest.

It is found that backscattering electric field ratio is much larger than 1 for some incident angles when there exists an overturning wave crest on the sea surface, which means a strong sea-spike phenomenon. While the backscattering electric field ratio is usually smaller than 1 when there is not an overturning wave crest, therefore the sea-spike phenomenon is difficult to take place in this situation. In other words, the overturning wave crest is one of the main reasons to sea spikes.

more complex overturning wave crest model.

ACKNOWLEDGMENT

This work was supported part by the National Natural Science Foundation of China (Grant No. 61701378), part by the China Postdoctoral Science Foundation (Grant No. 2017M613069), part by the Aeronautical Science Fund (Grant No. 20170181004), part by the Fundamental Research Funds for the Central Universities.

REFERENCES

- [1] L. B. Wetzel, *Electromagnetic Scattering from the Sea at Low Grazing Angles*. Surface Waves and Fluxes, vol. 8, pp. 109-171, 1990.
- [2] D. B. Trizna, "A model for Brewster angle damping and multipath effects on the microwave radar sea echo at low grazing angles," *IEEE Trans. Geosci. Remote Sens.*, vol. 35, no. 5, pp. 1232-1244, 1997.
- [3] J. C. West, "Low-grazing-angle (LGA) sea-spike backscattering from plunging breaker crests," *IEEE Trans. Geosci. Remote Sens.*, vol. 40, no. 2, pp. 523-526, 2002.
- [4] D. Holliday, L. L. DeRead, Jr., and G. J. St-Cyr,

- “Sea-spike backscatter from a steepening wave,” *IEEE Trans. Antennas Propagat.*, vol. 46, no. 1, pp. 108-113, 1998.
- [5] W. Yang, Z. Q. Zhao, C. H. Qi, et al., “Electromagnetic modeling of breaking waves at low grazing angles with adaptive higher order hierarchical Legendre basis functions,” *IEEE Trans. Geosci. Remote Sens.*, vol. 46, no. 1, pp. 346-352, 1998.
- [6] A. C. Patricio, C. H. Merrick, A. H. Robert, et al., “Optical and microwave detection of wave breaking in the surf zone,” *IEEE Trans. Geosci. Remote Sens.*, vol. 49, no. 6, pp. 1879-1893, 2011.
- [7] P. Wang, Y. Yao, and M. P. Tulin, “An efficient numerical tank for nonlinear water waves based on the multi-subdomain approach with B.E.M.,” *International Journal for Numerical Methods in Fluid*, vol. 20, no. 20, pp. 1315-1336, 1995.
- [8] I. T. Johnson, J. V. Toporkov, and G. S. Brown, “A numerical study of backscattering from time-evolving sea surfaces: Comparison of hydrodynamic models,” *IEEE Trans. Geosci. Remote Sens.*, vol. 39, no. 11, pp. 2411-2419, 2001.
- [9] A. K. Fung, Z. Q. Li, and K. S. Chen, “Backscattering from a randomly rough dielectric surface,” *IEEE Trans. Geosci. Remote Sens.*, vol. 30, no. 2, pp. 356-369, 1992.
- [10] R. F. Harrington and J. L. Harrington, *Field Computation by Moment Methods*. Macmillan, New York, 1968.
- [11] J. Li, L. X. Guo, Y. C. Jiao, et al., “Investigation on wide-band scattering of a 2-D target above 1-D randomly rough surface by FDTD method,” *Optics Express*, vol. 19, no. 2, pp. 1091-1100, 2011.
- [12] J. Song, C. C. Lu, and W. C. Chew, “Multilevel fast multiple algorithm for electromagnetic scattering by large complex objects,” *IEEE Trans. Antennas Propagat.*, vol. 45, no. 10, pp. 1488-1497, 1997.
- [13] J. Hu, et al., “Fast solution of electromagnetic scattering from thin dielectric coated PEC by MLFMM and successive over relaxation iterative technique,” *IEEE Microwave and Wireless Components Letters*, vol. 19, no. 12, pp. 762-764, 2009.
- [14] W. L. Li, L. X. Guo, X. Meng, et al., “Modeling and electromagnetic scattering from the overturning wave crest,” *Acta Phys. Sin.*, vol. 63, no. 16, pp. 164102-164102, 2014.
- [15] T. Elfouhaily, B. Chapron, K. Katsaros, et al., “A unified directional spectrum for long and short wind-driven waves,” *J. Geoph. Res.: Oceans (1978–2012)*, vol. 102, no. C7, pp. 15781-15796, 1997.
- [16] P. Debye, *Polar Molecules*. Chemical Catalog, New York, 1929.



Xiao Meng received the B.S. degree in Electronic Information Science and Technology from Xidian University, Xi’an, China in 2011. She is currently pursuing the Ph.D. degree at the School of Science.

Her research has been on electromagnetic scattering from rough sea surface and GPU high-performance computing in remote sensing and computational electromagnetics.



Li-xin Guo (S’95-M’03) received the M.S. degree in Radio Science from Xidian University, Xi’an, China, and the Ph.D degree in Astrometry and Celestial Mechanics from Chinese Academy of Sciences, China, in 1993 and 1999, respectively.

During 2001-2002 he was a Visiting Scholar at School of Electrical Engineering and Computer Science, Kyungpook National University, Korea. He has also held appointments as Visiting Professor at d’Energetique des Systemes et Precedes (LESP), University of Rouen, France and Faculty of Engineering and Physical Sciences, University of Manchester, England. He is currently a Professor and Head of School of Science at Xidian University, China. His research interests mainly includes: electromagnetic wave propagation and scattering in complex system, computational electromagnetic and fractal electrodynamics.

Guo is a Senior Member of Chinese Institute of Electronics (CIE) and a Fellow of Physics Institute of Shaanxi Province, China.